# Time-dependent active microrheology in dilute colloidal suspensions

Sebastian Leitmann,[1] Suvendu Mandal,[1] Matthias Fuchs,[2]
Antonio M. Puertas,[3] and Thomas Franosch[1,*]

[1]*Institut für Theoretische Physik, Universität Innsbruck, Technikerstraße 21A, A-6020 Innsbruck, Austria*
[2]*Fachbereich Physik, Universität Konstanz, 78457 Konstanz, Germany*
[3]*Group of Complex Fluids Physics, Department of Applied Physics, University of Almería, 04120 Almería, Spain*

(Received 20 October 2017; published 11 October 2018)

In a microrheological setup a single probe particle immersed in a complex fluid is exposed to a strong external force driving the system out of equilibrium. Here, we elaborate analytically the time-dependent response of a probe particle in a dilute suspension of Brownian particles to a large step force, exact in first order of the density of the bath particles. The time-dependent drift velocity approaches its stationary-state value exponentially fast for arbitrarily small driving in striking contrast to the power-law prediction of linear response encoded in the long-time tails of the velocity autocorrelation function. We show that the stationary-state behavior depends nonanalytically on the driving force and connect this behavior to the persistent correlations in the equilibrium state. We argue that this relation holds generically. Furthermore, we elaborate that the fluctuations in the direction of the force display transient superdiffusive behavior.

DOI: 10.1103/PhysRevFluids.3.103301

## I. INTRODUCTION

While the static and dynamic properties of interacting many-particle systems in equilibrium encode the linear response via the fluctuation-dissipation theorem, corresponding principles generally applicable for systems driven far from equilibrium remain a grand challenge in statistical physics. Soft matter systems are ideally suited to study such nonequilibrium phenomena, since their defining characteristic is that they are strongly susceptible to forces. Conceptually, the simplest experimentally realizable system then consists of an interacting colloidal suspension that is driven out of equilibrium by a strong external force acting on a single probe particle. This setup constitutes the basic paradigm for active microrheology with the principle goal to infer material properties beyond the linear regime [1–11].

The nonlinear mobility in the stationary state $\mu(\mathrm{Pe})$ for a suspension of interacting Brownian particles has been derived to first order of the density of bath particles $n$ in the seminal work by Squires and Brady [1] in terms of an asymptotic expansion

$$\mu(\mathrm{Pe})/\mu = 1 - \frac{2\pi n\sigma^3}{3}\frac{D_a}{D_r}\left[1 - \frac{2}{15}\mathrm{Pe}^2 + \frac{1}{8}|\mathrm{Pe}|^3 - \frac{128}{1575}\mathrm{Pe}^4 + O(|\mathrm{Pe}|^5)\right], \quad \mathrm{Pe}\to 0, \qquad (1)$$

where $\mu$ is the mobility of the probe particle at infinite dilution with diffusion coefficient $D_a$, and the Péclet number Pe is a suitable dimensionless measure for the driving force (see below). The motion of the bath particles with diffusion coefficient $D_b$ enters in terms of the diffusion coefficient of the relative motion, $D_r = D_a + D_b$.

*thomas.franosch@uibk.ac.at

 

The leading term of the corresponding asymptotic expansion of the fluctuations around the average drift has also been achieved [4], revealing a long-time diffusion coefficient that can become arbitrarily large for strong driving. Active microrheology has found fruitful applications in dense colloidal systems in the vicinity of the glass transition; in particular, computer simulations have revealed (transient) superdiffusion and enhanced diffusivities [12,13]. Certain phenomena in the nonlinear regime have also been rationalized within a mode-coupling approach [14–20], continuous-time random walks [21–24], Langevin equations [25,26], and kinetic theory [27].

Exact results beyond the stationary state have been accomplished for driven transport in lattice models, e.g., for a biased intruder in a dense crowded environment of mobile hard-core obstacles [28–33] and the complementary limit of a tracer in a dilute quenched array of obstacles [34–36]. Due to repeated encounters with the same obstacle, one finds that the nonlinear force-dependent mobility in the stationary state becomes a nonanalytic function of the driving force.

For the case of colloids in continuum, one infers that the mobility also becomes a nonanalytic function in the Péclet number, signaled by $|\mathrm{Pe}|^3$ in the asymptotic expansion [Eq. (1)], since the mobility has to be an even function of Pe.

The frequency-dependent linear mobility $\hat{\mu}(\omega)$ can be obtained via the fluctuation-dissipation theorem from the velocity-autocorrelation function in equilibrium, which has been calculated earlier to the same order in the packing fraction [37–41]

$$-i\omega\hat{\mu}(\omega)/\mu = 1 - \frac{2\pi n\sigma^3}{3}\frac{D_a}{D_r}\frac{1+\sqrt{-i\omega\tau}}{1+\sqrt{-i\omega\tau}-i\omega\tau/2}, \tag{2}$$

with diffusive time scale $\tau = \sigma^2/D_r$. Here, the nonanalytic contribution in the frequency $\omega$ reflects the well-known long-time tail in the velocity-autocorrelation function $Z(t) \simeq -At^{-5/2}$, $A > 0$, also familiar from the Lorentz model [42–47].

These results immediately raise the following questions: How do the nonanalytic contributions in the nonlinear mobility emerge from a perturbative scheme and are they related to the persistent correlations in equilibrium? How fast is the nonequilibrium steady state approached from an initial equilibrium state in comparison to the predictions of linear response? What is the intermediate time-dependent behavior of the fluctuations connecting the short-time motion to the drastically enhanced long-time diffusion? These questions are answered by solving the two-particle Smoluchowski equation for the time-dependent dynamics in the presence of a strong force. Thereby, we unify the previous approaches for the driven stationary state [1,4] and the time-dependent equilibrium dynamics [37–40] and reveal the interplay between persistent correlations and nonequilibrium driving. The solution enables us to fully address the time-dependent approach to the stationary state, in principle for all moments of the displacement along the force. The two lowest moments, the mobility and the fluctuations, are elaborated and compared to computer simulations.

This work is organized as follows. In Sec. II the underlying model is introduced followed by the complete solution strategy. The main result of this section is the self-energy encoding the dynamics between the probe and the bath particles. Readers who are primarily concerned about the results may skip this section and jump directly to Sec. III, where we determine the time-dependent behavior in terms of the mobility and the fluctuations along the applied force. The obtained results from the analytic solution are compared to computer simulations and the phenomena involved in the transition from the initial equilibrium state to the new stationary state are discussed. In Sec. IV, the key results of this work are summarized followed by general conclusions. In the appendix, we present the details of the simulations used to test the theory.

## II. MODEL AND SOLUTION STRATEGY

We solve for the time-dependent dynamics of a probe particle pulled by a force in the presence of other bath particles. In first order of the density of bath particles, the dynamics is completely encoded by the interactions of the probe particle with a single bath particle [1,48]. Discarding inertial effects it is sufficient to consider the two-particle Smoluchowski equation for probe and bath particle. The

problem can be expressed via the independent motion of the center of diffusion and the relative distance between both particles. The dynamics of the relative distance is described in the frequency domain in terms of a self-energy which encodes all corrections to the dynamics of the probe particle due to interactions.

### A. Two-particle Smoluchowski equation

We consider a single probe particle $a$ interacting with a bath particle $b$ with bare diffusion coefficients $D_a$ and $D_b$, respectively. The particles interact by mutual hard-core exclusion with exclusion distance $\sigma$. At time $t = 0$ an external constant force $\vec{F}$ is switched on, pulling the probe particle and driving the system from its initial equilibrium state into a nonequilibrium stationary state. We describe the state of the system by the conditional probability density $\Psi(\vec{r}_a, \vec{r}_b, t|\vec{r}_a', \vec{r}_b')$ for probe particle $a$ and bath particle $b$ to be at positions $\vec{r}_a$, $\vec{r}_b$ at time $t$ provided they start at initial positions $\vec{r}_a'$, $\vec{r}_b'$ at time $t = 0$. Since the system is initially in equilibrium, the corresponding initial condition reads $\Psi(\vec{r}_a, \vec{r}_b, t = 0|\vec{r}_a', \vec{r}_b') = \vartheta(|\vec{r}_a' - \vec{r}_b'| - \sigma)\delta(\vec{r}_a - \vec{r}_a')\delta(\vec{r}_b - \vec{r}_b')/V$, where the Heaviside function $\vartheta(\cdot)$ accounts for the mutual exclusion. The limit of large box sizes $V \to \infty$ is anticipated throughout. At time $t = 0$, the force $\vec{F}$ is switched on and the probability density evolves according to the Smoluchowski equation,

$$\partial_t \Psi = \left(D_a \nabla_a^2 + D_b \nabla_b^2\right)\Psi - \mu \vec{F} \cdot \vec{\nabla}_a \Psi, \tag{3}$$

with bare mobility $\mu = D_a/k_\mathrm{B}T$ of the probe particle and the thermal scale $k_\mathrm{B}T$. The hard-core interaction between probe and bath particle is encoded in the no-flux boundary condition

$$(\vec{r}_a - \vec{r}_b) \cdot [\mu \vec{F} \Psi - (D_a \vec{\nabla}_a - D_b \vec{\nabla}_b)\Psi] = 0, \quad \text{for } |\vec{r}_a - \vec{r}_b| = \sigma. \tag{4}$$

We introduce new coordinates for the center of diffusion, $\vec{R} = (D_b \vec{r}_a + D_a \vec{r}_b)/(D_a + D_b)$, and the relative distance $\vec{r} = \vec{r}_a - \vec{r}_b$. After transformation, the Smoluchowski equation in these adapted coordinates reads

$$\partial_t \Psi = \frac{D_a D_b}{D_r} \nabla_R^2 \Psi - \frac{\mu D_b}{D_r} \vec{F} \cdot \vec{\nabla}_R \Psi + D_r \nabla_r^2 \Psi - \mu \vec{F} \cdot \vec{\nabla}_r \Psi, \tag{5}$$

with the diffusion coefficient for the relative motion, $D_r = D_a + D_b$. Similarly, the no-flux boundary condition transforms to

$$\vec{r} \cdot [\mu \vec{F} \Psi - D_r \vec{\nabla}_r \Psi] = 0, \quad \text{for } |\vec{r}| = \sigma. \tag{6}$$

The Smoluchowski equation and the no-flux boundary condition in the new coordinates [Eqs. (5) and (6)] reveal that the motion of the center of diffusion $\vec{R}$ and the dynamics of the relative motion, $\vec{r}$, are independent. Thus, the conditional probability factorizes into a simple Gaussian with diffusion coefficient $D_a D_b/D_r$ and drift $\mu \vec{F} D_b/D_r$ for the center of diffusion $\vec{R}$, and the conditional probability $\psi(\vec{r}, t|\vec{r}\,')$ to find relative distances $\vec{r}$ and $\vec{r}\,'$ at times $t$ and 0, respectively. It fulfills the reduced Smoluchowski equation

$$\partial_t \psi = D_r \nabla_r^2 \psi - \mu \vec{F} \cdot \vec{\nabla}_r \psi, \tag{7}$$

and the initial condition is provided by the equilibrium state $\psi(\vec{r}, t = 0|\vec{r}\,') = \vartheta(|\vec{r}\,'| - \sigma)\delta(\vec{r} - \vec{r}\,')$. Similarly, the no-flux boundary condition for the conditional probability $\psi$ reads

$$\vec{r} \cdot [\mu \vec{F} \psi - D_r \vec{\nabla}_r \psi] = 0, \quad \text{for } |\vec{r}| = \sigma. \tag{8}$$

It is natural to measure the force in terms of the dimensionless Péclet number $\mathrm{Pe} = \mu F \sigma/D_r$ that already appeared in Eq. (1) [1,4], which can be written also as $\mathrm{Pe} = (F\sigma/k_\mathrm{B}T)D_a/D_r$ by using the Stokes-Einstein relation. This definition encompasses the case of equal-sized colloids, $\mathrm{Pe} = F\sigma/2k_\mathrm{B}T$, as well as the Lorentz model, $\mathrm{Pe} = F\sigma/k_\mathrm{B}T$, where the bath particles are fixed in space ($D_b = 0$).

Our main quantity of interest is the intermediate scattering function $\langle e^{-i\vec{q}\cdot\Delta\vec{r}_a(t)}\rangle$ for the displacement $\Delta\vec{r}_a(t) = \vec{r}_a(t) - \vec{r}_a(0)$ of the probe particle, from which in principle all moments of the displacement can be extracted by derivatives with respect to the wave vector $\vec{q}$. In the new coordinates, $\Delta\vec{r}_a(t) = \Delta\vec{R}(t) + D_a\Delta\vec{r}(t)/D_r$, the intermediate scattering function can be expressed as

$$\langle e^{-i\vec{q}\cdot\Delta\vec{r}_a(t)}\rangle = \langle e^{-i\vec{q}\cdot\Delta\vec{R}(t)}\rangle\langle e^{-i(D_a/D_r)\vec{q}\cdot\Delta\vec{r}(t)}\rangle, \tag{9}$$

where we used the independence of $\vec{R}$ and $\vec{r}$ [Eq. (5)]. Since the dynamics of the center of diffusion is Gaussian with diffusion coefficient $D_aD_b/D_r$ and drift $\mu\vec{F}D_b/D_r$, one finds immediately

$$\langle e^{-i\vec{q}\cdot\Delta\vec{R}(t)}\rangle = e^{-i\vec{q}\cdot(\mu\vec{F}D_b/D_r)t}e^{-q^2(D_aD_b/D_r)t}. \tag{10}$$

The remaining task is the calculation of the intermediate scattering function $\langle e^{-i(D_a/D_r)\vec{q}\cdot\Delta\vec{r}(t)}\rangle$ for the relative motion $\Delta\vec{r}(t)$ between probe and bath particle.

### B. Dynamics of the relative motion

This part contains the detailed calculation of the relative motion and contains the heart of our analytic approach. The solution strategy is adapted from Felderhof and Jones' approach for the equilibrium dynamics [40].

The intermediate scattering function, viz., the characteristic function of the relative displacement $\Delta\vec{r}(t) = \vec{r}(t) - \vec{r}(0)$,

$$\langle e^{-i\vec{q}\cdot\Delta\vec{r}(t)}\rangle = \int d^3r \int \frac{d^3r'}{V}\, e^{-i\vec{q}\cdot(\vec{r}-\vec{r}\,')}\psi(\vec{r},t|\vec{r}\,'), \tag{11}$$

allows extracting the moments by series expansion in the wave vector $\vec{q}$. To make analytic progress, we only consider the axially symmetric case, where the wave vector and force are aligned: $\vec{q} \parallel \vec{F}$. This enables us to determine the motion in the direction of the force; the time-dependent motion perpendicular to the force is left for future analysis. We perform a temporal Fourier-Laplace transform and a spatial Fourier transform,

$$\hat{\psi}_q(\vec{r},\omega) := \int_0^\infty dt\, e^{i\omega t}\int \frac{d^3r'}{\sqrt{V}}\, e^{i\vec{q}\cdot\vec{r}\,'}\psi(\vec{r},t|\vec{r}\,'). \tag{12}$$

The transformed quantity $\hat{\psi}_q(\vec{r},\omega)$ is connected to the propagator $G(q,\omega)$ via a spatial Fourier transform $G(q,\omega) := \int d^3r\, e^{-i\vec{q}\cdot\vec{r}}\hat{\psi}_q(\vec{r},\omega)/\sqrt{V}$. From Eq. (7) and the initial condition one derives the equation of motion [40]

$$(-i\omega - D_r\nabla^2 + \mu\vec{F}\cdot\vec{\nabla})\hat{\psi}_q = \frac{1}{\sqrt{V}}e^{i\vec{q}\cdot\vec{r}}\vartheta(|\vec{r}| - \sigma). \tag{13}$$

In particular, $\hat{\psi}_q(\vec{r},\omega) = 0$ for $|\vec{r}| < \sigma$ reflects the hard-core exclusion. Without interaction, we denote the respective conditional probability by $\hat{\psi}_q^0$ which evolves according to

$$(-i\omega - D_r\nabla^2 + \mu\vec{F}\cdot\vec{\nabla})\hat{\psi}_q^0 = \frac{1}{\sqrt{V}}e^{i\vec{q}\cdot\vec{r}}. \tag{14}$$

The free motion allows for a plane-wave solution of the form

$$\hat{\psi}_q^0(\vec{r},\omega) = \frac{e^{i\vec{q}\cdot\vec{r}}/\sqrt{V}}{-i\omega + D_rq^2 + i\mu Fq}, \tag{15}$$

which is valid for all $\vec{r} \in V$, and the respective free propagator can be read off as

$$G_0(q,\omega) = \frac{1}{-i\omega + D_rq^2 + i\mu Fq}. \tag{16}$$

In particular, the plane-wave solution can be written as $\hat{\psi}_q^0(\vec{r},\omega) = G_0(q,\omega)e^{i\vec{q}\cdot\vec{r}}/\sqrt{V}$. To make further progress, we observe that the difference of Eqs. (13) and (14),

$$(-i\omega - D_r\nabla^2 + \mu\vec{F}\cdot\vec{\nabla})\big[\hat{\psi}_q(\vec{r},\omega) - \hat{\psi}_q^0(\vec{r},\omega)\big] = 0, \quad \text{for } |\vec{r}| > \sigma, \tag{17}$$

vanishes for terminal distance $|\vec{r}|$ larger than the exclusion distance $\sigma$. We are interested in the forward-scattering amplitude

$$G(q,\omega) - G_0(q,\omega) = \frac{1}{\sqrt{V}}\int d^3r\; e^{-i\vec{q}\cdot\vec{r}}\big[\hat{\psi}_q(\vec{r},\omega) - \hat{\psi}_q^0(\vec{r},\omega)\big], \tag{18}$$

which we separate into contributions outside and inside of the region of overlap of probe and bath particle:

$$\begin{aligned} G(q,\omega) - G_0(q,\omega) = {} & \frac{1}{\sqrt{V}}\int_{|\vec{r}|>\sigma} d^3r\; e^{-i\vec{q}\cdot\vec{r}}\big[\hat{\psi}_q(\vec{r},\omega) - \hat{\psi}_q^0(\vec{r},\omega)\big] \\ & + \frac{1}{\sqrt{V}}\int_{|\vec{r}|<\sigma} d^3r\; e^{-i\vec{q}\cdot\vec{r}}\big[\hat{\psi}_q(\vec{r},\omega) - \hat{\psi}_q^0(\vec{r},\omega)\big]. \end{aligned} \tag{19}$$

In the second term we observe that the conditional probability $\hat{\psi}_{\vec{q}}$ vanishes for terminal positions inside the obstacle. Hence, there we can immediately compute the integral

$$\frac{1}{\sqrt{V}}\int_{|\vec{r}|<\sigma} d^3r\; e^{-i\vec{q}\cdot\vec{r}}\hat{\psi}_q^0(\vec{r},\omega) = \frac{4\pi\sigma^3/3V}{-i\omega + D_r q^2 + i\mu F q}. \tag{20}$$

To calculate the first term in Eq. (19), it is advantageous to convert the volume integral into a surface integral relying on the equations of motion. We use the auxiliary variable $\chi(\vec{r}) = \hat{\psi}_q(\vec{r},\omega) - \hat{\psi}_q^0(\vec{r},\omega)$ and investigate the identity

$$\int_{|\vec{r}|>\sigma} d^3r\; e^{-i\vec{q}\cdot\vec{r}}(-i\omega - D_r\nabla^2 + \mu\vec{F}\cdot\vec{\nabla})\chi(\vec{r}) = 0, \tag{21}$$

which follows from Eq. (17). Then, for the drift, we obtain

$$\begin{aligned} & \int_{|\vec{r}|>\sigma} d^3r\; e^{-i\vec{q}\cdot\vec{r}}(-\mu\vec{F}\cdot\vec{\nabla})\chi(\vec{r}) \\ & = \int_{|\vec{r}|>\sigma} d^3r\; (-\mu\vec{F}\cdot\vec{\nabla})[e^{-i\vec{q}\cdot\vec{r}}\chi(\vec{r})] + \int_{|\vec{r}|>\sigma} d^3r\; \chi(\vec{r})\mu\vec{F}\cdot\vec{\nabla}e^{-i\vec{q}\cdot\vec{r}} \\ & = \int dS_{\vec{r}}\,\hat{\vec{r}}\cdot\mu\vec{F}e^{-i\vec{q}\cdot\vec{r}}\chi(\vec{r}) + \int_{|\vec{r}|>\sigma} d^3r\; \chi(\vec{r})\mu\vec{F}\cdot\vec{\nabla}e^{-i\vec{q}\cdot\vec{r}}, \end{aligned} \tag{22}$$

where we introduced the unit vector $\hat{\vec{r}} = \vec{r}/|\vec{r}|$ and the surface element $dS_{\vec{r}}$ of the sphere of radius $\sigma$. Similarly, for the diffusive contribution, we derive

$$\begin{aligned} & \int_{|\vec{r}|>\sigma} d^3r\; e^{-i\vec{q}\cdot\vec{r}} D_r\nabla^2\chi(\vec{r}) \\ & = \int_{|\vec{r}|>\sigma} d^3r\; D_r\vec{\nabla}\cdot[e^{-i\vec{q}\cdot\vec{r}}\vec{\nabla}\chi(\vec{r})] - \int_{|\vec{r}|>\sigma} d^3r\; [D_r\vec{\nabla}\chi(\vec{r})]\cdot\vec{\nabla}e^{-i\vec{q}\cdot\vec{r}} \\ & = -\int dS_{\vec{r}}\; D_r\hat{\vec{r}}\cdot e^{-i\vec{q}\cdot\vec{r}}\vec{\nabla}\chi(\vec{r}) - \int_{|\vec{r}|>\sigma} d^3r\; D_r\vec{\nabla}\cdot[\chi(\vec{r})\;\vec{\nabla}e^{-i\vec{q}\cdot\vec{r}}] + \int_{|\vec{r}|>\sigma} d^3r\; \chi(\vec{r})D_r\nabla^2 e^{-i\vec{q}\cdot\vec{r}} \\ & = -\int dS_{\vec{r}}\; D_r\hat{\vec{r}}\cdot e^{-i\vec{q}\cdot\vec{r}}\vec{\nabla}\chi(\vec{r}) + \int dS_{\vec{r}}\; D_r\hat{\vec{r}}\cdot[\chi(\vec{r})\;\vec{\nabla}e^{-i\vec{q}\cdot\vec{r}}] + \int_{|\vec{r}|>\sigma} d^3r\; \chi(\vec{r})D_r\nabla^2 e^{-i\vec{q}\cdot\vec{r}}. \end{aligned} \tag{23}$$

Together, this yields

$$(-i\omega + D_r q^2 + i\mu\vec{F}\cdot\vec{q}) \int_{|\vec{r}|>\sigma} d^3\vec{r}\ \chi(\vec{r}) e^{-i\vec{q}\cdot\vec{r}}$$
$$= \int dS_{\vec{r}}\, \hat{\vec{r}} \cdot [\mu\vec{F}\chi(\vec{r}) - D_r\vec{\nabla}\chi(\vec{r})] e^{-i\vec{q}\cdot\vec{r}} + \int dS_{\vec{r}}\, D_r \hat{\vec{r}} \cdot [\chi(\vec{r})\, \vec{\nabla} e^{-i\vec{q}\cdot\vec{r}}]. \tag{24}$$

The first term on the right-hand side simplifies by the no-flux boundary condition [Eq. (8)] and the plane-wave solution $\hat{\psi}_q^0$ [Eq. (15)]:

$$\begin{aligned}\int dS_{\vec{r}}\, \hat{\vec{r}} \cdot [\mu\vec{F}\chi - D_r\vec{\nabla}\chi] e^{-i\vec{q}\cdot\vec{r}} &= -\int dS_{\vec{r}}\, e^{-i\vec{q}\cdot\vec{r}} \hat{\vec{r}} \cdot [\mu\vec{F} - D_r\vec{\nabla}] \hat{\psi}_{\vec{q}}^0(\vec{r},\omega) \\ &= -\int dS_{\vec{r}}\, e^{-i\vec{q}\cdot\vec{r}} \hat{\vec{r}} \cdot [\mu\vec{F} - iD_r\vec{q}] \hat{\psi}_{\vec{q}}^0(\vec{r},\omega) \\ &= \frac{-1/\sqrt{V}}{-i\omega + D_r q^2 + i\mu\vec{F}\cdot\vec{q}} \int dS_{\vec{r}}\, \hat{\vec{r}} \cdot [\mu\vec{F} - iD_r\vec{q}] = 0, \end{aligned} \tag{25}$$

where in the last line the flux integral of a constant vector vanishes. Collecting results, we obtain an expression for the forward-scattering amplitude in terms of a surface integral of the difference of the conditional probabilities:

$$G(q,\omega) - G_0(q,\omega) = G_0(q,\omega)\left\{-\frac{4\pi\sigma^3}{3V} - \frac{1}{\sqrt{V}} \int dS_{\vec{r}}\, iD_r\vec{q}\cdot\hat{\vec{r}} e^{-i\vec{q}\cdot\vec{r}} \left[\hat{\psi}_q(\vec{r},\omega) - \hat{\psi}_q^0(\vec{r},\omega)\right]\right\}. \tag{26}$$

In order to determine the conditional probabilities, we return to Eq. (17). For the solution of the homogeneous part of Eq. (17), we use the imaginary "gauge transformation" $\hat{X}(\vec{r},\omega) = [\hat{\psi}_q(\vec{r},\omega) - \hat{\psi}_q^0(\vec{r},\omega)] e^{-\mu\vec{F}\cdot\vec{r}/2D_r}$ such that the drift term is absorbed in the Laplacian by completing the square, $\vec{\nabla} \to \vec{\nabla} - \mu\vec{F}/2D_r$ [1,49]. This step will have crucial implications for the results at finite forces. Then, the new quantity $\hat{X}$ fulfills the three-dimensional source-free Helmholtz equation

$$(\kappa^2 - \nabla^2)\hat{X}(\vec{r},\omega) = 0, \quad \text{for } |\vec{r}| > \sigma, \tag{27}$$

with complex wave number $\kappa^2\sigma^2 = -i\omega\tau + (\mathrm{Pe}/2)^2$ and diffusive time scale $\tau = \sigma^2/D_r$. We write the general axially symmetric solution in the form

$$\hat{\psi}_q(\vec{r},\omega) - \hat{\psi}_q^0(\vec{r},\omega) = \frac{e^{\mu\vec{F}\cdot\vec{r}/2D_r}/\sqrt{V}}{-i\omega + D_r q^2 + i\mu F q} \sum_{\ell=0}^{\infty} a_\ell \frac{\mathrm{k}_\ell(\kappa r)}{\mathrm{k}_\ell(\kappa\sigma)} \mathrm{P}_\ell(\cos\vartheta), \tag{28}$$

for $|\vec{r}| > \sigma$, with modified spherical Bessel functions of the second kind $\mathrm{k}_\ell(\cdot)$ and Legendre polynomials $\mathrm{P}_\ell(\cdot)$.

The expansion coefficients $a_\ell$ for the different angular channels $\ell$ have to be determined via the no-flux boundary condition [Eq. (8)]:

$$\left[\mu F\cos\vartheta - D_r\frac{\partial}{\partial r}\right]\left(\hat{\psi}_q - \hat{\psi}_q^0\right)\Big|_{r=\sigma} = -\left[\mu F\cos\vartheta - D_r\frac{\partial}{\partial r}\right]\hat{\psi}_q^0\Big|_{r=\sigma}. \tag{29}$$

With the explicit solutions [Eqs. (15) and (28)], we find that the expansion coefficients $a_\ell$ have to fulfill

$$\left[\mathrm{Pe}\,\eta - \sigma\frac{\partial}{\partial r}\right] e^{\mathrm{Pe}\,\eta r/2\sigma} \sum_{\ell=0}^{\infty} a_\ell \frac{\mathrm{k}_\ell(\kappa r)}{\mathrm{k}_\ell(\kappa\sigma)} \mathrm{P}_\ell(\eta)|_{r=\sigma} = -\left[\mathrm{Pe}\,\eta - \sigma\frac{\partial}{\partial r}\right] e^{iq\eta r}|_{r=\sigma}, \tag{30}$$

where we abbreviated $\eta = \cos(\vartheta)$ and used the Péclet number $\mathrm{Pe} = \mu F \sigma / D_r$. Performing the derivatives, the relation can be expressed as

$$\begin{aligned} e^{-\mathrm{Pe}\,\eta/2}(\mathrm{Pe} - iq\sigma)\eta e^{iq\sigma\eta} &= \sum_{\ell=0}^{\infty} a_\ell \left[\frac{\kappa\sigma \mathrm{k}'_\ell(\kappa\sigma)}{\mathrm{k}_\ell(\kappa\sigma)} - \frac{\mathrm{Pe}}{2}\eta\right]\mathrm{P}_\ell(\eta) \\ &= \sum_{\ell=0}^{\infty}\left[\frac{\kappa\sigma \mathrm{k}'_\ell(\kappa\sigma)}{\mathrm{k}_\ell(\kappa\sigma)} a_\ell \mathrm{P}_\ell(\eta) - \frac{\mathrm{Pe}}{2} a_\ell \left(\frac{\ell+1}{2\ell+1}\mathrm{P}_{\ell+1}(\eta) + \frac{\ell}{2\ell+1}\mathrm{P}_{\ell-1}(\eta)\right)\right] \\ &= \sum_{\ell=0}^{\infty}\left[\frac{\kappa\sigma \mathrm{k}'_\ell(\kappa\sigma)}{\mathrm{k}_\ell(\kappa\sigma)} a_\ell - \frac{\mathrm{Pe}}{2}\frac{\ell}{2\ell-1} a_{\ell-1} - \frac{\mathrm{Pe}}{2}\frac{\ell+1}{2\ell+3} a_{\ell+1}\right]\mathrm{P}_\ell(\eta), \end{aligned} \tag{31}$$

where we used the recursion formula $(\ell+1)\mathrm{P}_{\ell+1}(\eta) = (2\ell+1)\eta\mathrm{P}_\ell(\eta) - \ell\mathrm{P}_{\ell-1}(\eta)$. Using the orthogonality relation of the Legendre polynomials, $\int_{-1}^{1} d\eta\ \mathrm{P}_\ell(\eta)\mathrm{P}_{\ell'}(\eta) = 2\delta_{\ell\ell'}/(2\ell+1)$, this becomes a tridiagonal matrix equation:

$$\frac{\kappa\sigma \mathrm{k}'_\ell(\kappa\sigma)}{\mathrm{k}_\ell(\kappa\sigma)} a_\ell - \frac{\mathrm{Pe}}{2}\frac{\ell}{2\ell-1} a_{\ell-1} - \frac{\mathrm{Pe}}{2}\frac{\ell+1}{2\ell+3} a_{\ell+1} = b_\ell. \tag{32}$$

The inhomogeneity $b_\ell$ is defined as

$$b_\ell = \frac{2\ell+1}{2}(\mathrm{Pe} - iq\sigma)\int_{-1}^{1} d\eta\ \eta \mathrm{P}_\ell(\eta) e^{-\mathrm{Pe}\,\eta/2} e^{iq\sigma\eta}. \tag{33}$$

The remaining integral can be solved using the Rayleigh identity $e^{-iz\cos\vartheta} = \sum_{\ell=0}^{\infty}(-i)^\ell(2\ell+1)\mathrm{j}_\ell(z)\mathrm{P}_\ell(\cos\vartheta)$, with spherical Bessel function $\mathrm{j}_\ell(\cdot)$ and relying again on the orthogonality relation of the Legendre polynomials:

$$b_\ell = -(2\ell+1)(q\sigma + i\mathrm{Pe})i^\ell \mathrm{j}'_\ell(q\sigma + i\mathrm{Pe}/2), \tag{34}$$

where the prime indicates a derivative. For the special case of vanishing wave number $q = 0$ and the stationary state $\omega = 0$, we recover the tridiagonal matrix derived in Ref. [1].

For the forward-scattering amplitude [Eq. (26)], we calculate the integral over the spherical surface with radius $r = \sigma$:

$$\begin{aligned} &\frac{1}{\sqrt{V}}\int dS_{\vec{r}}\, i D_r \vec{q}\cdot\hat{\vec{r}} e^{-i\vec{q}\cdot\vec{r}}\left[\hat{\psi}_q(\vec{r},\omega) - \hat{\psi}^0_q(\vec{r},\omega)\right] \\ &\quad = \frac{2\pi i D_r \sigma^2 q/V}{-i\omega + D_r q^2 + i\mu F q}\sum_{\ell=0}^{\infty} a_\ell \int_{-1}^{1} d\eta\,\eta e^{-iq\sigma\eta} e^{\mu F\sigma\eta/2D_r}\mathrm{P}_\ell(\eta). \end{aligned} \tag{35}$$

The integral on the right-hand side can be evaluated again by inserting the Rayleigh identity. As a result, we find

$$\int_{-1}^{1} d\eta\,\eta e^{-iq\sigma\eta} e^{\eta\mathrm{Pe}/2}\mathrm{P}_\ell(\eta) = \frac{\partial}{\partial(\mathrm{Pe}/2)}\int_{-1}^{1} d\eta\, e^{-iq\sigma\eta} e^{\eta\mathrm{Pe}/2}\mathrm{P}_\ell(\eta) = 2i(-i)^\ell \mathrm{j}'_\ell(q\sigma + i\mathrm{Pe}/2). \tag{36}$$

Collecting results, one finds

$$G(q,\omega) - G_0(q,\omega) = -\frac{4\pi\sigma^3}{3V}G_0(q,\omega) + \frac{4\pi D_r\sigma^2 q}{V}G_0(q,\omega)^2\sum_{\ell=0}^{\infty} a_\ell(-i)^\ell \mathrm{j}'_\ell(q\sigma + i\mathrm{Pe}/2). \tag{37}$$

The first term on the right-hand side merely reflects that the free propagator $G_0(q,\omega) = (-i\omega + D_r q^2 + i\mu F q)^{-1}$ allows for particles starting also inside of the obstacle, thereby renormalizing the residue of the perturbed propagator. We may safely drop this term. Conventionally, the result is expressed in terms of a self-energy $\Sigma(q,\omega)$ via the Dyson equation $G = G_0 + G_0\Sigma G$. To first

order in the density, the self-energy is merely proportional to the number density $n = N/V$ of the bath particles, and we obtain the self-energy as our main result of the analytic calculations:

$$\Sigma(q,\omega) = 4\pi n D_r \sigma^2 q \sum_{\ell=0}^{\infty} a_\ell (-i)^\ell \mathrm{j}'_\ell(q\sigma + i\mathrm{Pe}/2). \tag{38}$$

The self-energy encodes the density-induced corrections of all moments of the relative motion along the force. The leading factor $q$ reflects the particle-conservation law.

Without external driving, $\mathrm{Pe} = 0$, the tridiagonal matrix for the coefficients $a_\ell$ [Eq. (32)] becomes diagonal, yielding

$$a_\ell = -(2\ell+1) q\sigma i^\ell \mathrm{j}'_\ell(q\sigma) \frac{\mathrm{k}_\ell(\kappa\sigma)}{\kappa\sigma \mathrm{k}'_\ell(\kappa\sigma)}. \tag{39}$$

Thus, we recover the known result for the self-energy for equilibrium [37–40]:

$$\Sigma(q,\omega) = -4\pi n D_r \sigma^3 q^2 \sum_{\ell=0}^{\infty} (2\ell+1) [\mathrm{j}'_\ell(q\sigma)]^2 \frac{\mathrm{k}_\ell(\kappa\sigma)}{\kappa\sigma \mathrm{k}'_\ell(\kappa\sigma)}. \tag{40}$$

In the case of driving, only terms of order $\ell = O(\mathrm{Pe})$ significantly contribute for small wave numbers and the matrix [Eq. (32)] may be safely truncated for numerical evaluation. The matrix inversion does not generate nonanalytic behavior and one infers that the coefficients $a_\ell \equiv a_\ell(q\sigma, \kappa\sigma, \mathrm{Pe})$ should be analytic functions in the arguments. In particular, the matrix is suited for a perturbative approach for small Péclet numbers; in particular, the linear response results can be derived.

The matrix in Eq. (32) determines the coefficients $a_\ell$ and thereby the complete solution of the self-energy [Eq. (38)]. Up to matrix inversion and a temporal Fourier back-transform, which have to be implemented numerically, we have elaborated a complete time-dependent analytic solution for the relative motion of the probe particle in the presence of bath particles for the dilute case.

## III. CUMULANTS OF THE DISPLACEMENT

The intermediate scattering function generates the moments of the displacement along the field by taking derivatives with respect to the wave number. In this section we elaborate explicitly how the mean displacement, respectively the time-dependent nonlinear mobility, and the fluctuations along the field can be calculated from the self-energy of the relative motion.

The starting point is the intermediate scattering functions for the displacement [Eqs. (9) and (10)], where we put the wave vector along the field, $\vec{q} \| \vec{F}$, which is chosen as the $z$ direction. The corresponding cumulant generating function is obtained by taking the logarithm:

$$\begin{aligned} \ln\langle e^{-iq\Delta z_a(t)}\rangle &= \ln\langle e^{-iq\Delta Z(t)}\rangle + \ln\langle e^{-i(D_a q/D_r)\Delta z(t)}\rangle \\ &= -iq(\mu F D_b/D_r)t - q^2(D_a D_b/D_r)t + \ln\langle e^{-i(D_a q/D_r)\Delta z(t)}\rangle. \end{aligned} \tag{41}$$

This formula establishes the connection between the relative motion $z(t)$ and the displacement of the probe particle, $z_a(t)$.

### A. Average motion

First, we discuss the time-dependent nonlinear mobility defined by

$$\mu(t, \mathrm{Pe}) := \frac{1}{F}\frac{d}{dt}\langle \Delta z_a(t)\rangle, \tag{42}$$

characterizing the mean motion of the probe particle, upon switching on the force in the $z$ direction. From the cumulant generating function of the displacement $\Delta z_a(t)$ [Eq. (41)], the mean

displacement $\langle \Delta z_a(t)\rangle$ is obtained as

$$\langle \Delta z_a(t)\rangle = i\frac{\partial}{\partial q}\ln\langle e^{-iq\Delta z_a(t)}\rangle|_{q=0} = \mu F t D_b/D_r + \frac{iD_a}{D_r}\frac{\partial}{\partial(D_a q/D_r)}\ln\langle e^{-i(D_a q/D_r)\Delta z(t)}\rangle|_{q=0}$$
$$= \mu F t D_b/D_r + \frac{D_a}{D_r}\langle \Delta z(t)\rangle. \tag{43}$$

The contribution from the relative motion can be obtained from the intermediate scattering function [Eq. (11)] as the first derivative $\partial/\partial q|_{q=0}$. The dynamics of the relative distance $\Delta z(t)$ between probe and bath particle is contained in the propagator

$$G(q,\omega) = G_0(q,\omega) + G_0(q,\omega)^2\Sigma(q,\omega) + O(n)^2, \tag{44}$$

with free propagator $G_0(q,\omega) = (-i\omega + D_r q^2 + iq\mu F)^{-1}$ and self-energy $\Sigma(q,\omega)$ [Eq. (38)]. Taking the $q$ derivative leads to the appearance of the frequency-dependent expression $\mathcal{L}\{\langle\Delta z(t)\rangle\}(\omega) := \int_0^\infty dt\ e^{i\omega t}\langle\Delta z(t)\rangle$. It is obtained by considering the propagator $G(q,\omega)$ [Eq. (44)]:

$$\mathcal{L}\{\langle\Delta z(t)\rangle\}(\omega) = i\frac{\partial}{\partial q}G(q,\omega)|_{q=0} = \left[i\frac{\partial G_0}{\partial q} + iG_0^2\frac{\partial\Sigma}{\partial q}\right]_{q=0}$$
$$= \frac{\mu F}{(-i\omega)^2} + 2\pi n\sigma^3\frac{\mu F}{(-i\omega)^2}\sum_{\ell=0}^{\infty} a_\ell\frac{\mathrm{i}'_\ell(\mathrm{Pe}/2)}{\mathrm{Pe}/2}, \tag{45}$$

where, in the second line, we used the relation $D_r/\sigma = \mu F/\mathrm{Pe}$ and expressed the spherical Bessel functions $\mathrm{j}_\ell(\cdot)$ in terms of $(-i)\mathrm{i}'_\ell(\mathrm{Pe}/2) = (-i)^\ell \mathrm{j}'_\ell(i\mathrm{Pe}/2)$ with modified spherical Bessel function $\mathrm{i}_\ell(\cdot)$. The coefficients $a_\ell = a_\ell(q\sigma, \kappa\sigma, \mathrm{Pe})$ are to be evaluated for vanishing wave number $q = 0$. In the above equation, the first term corresponds to the free motion and the second encodes the density-induced response. Then, the mean displacement of the probe particle along the field, $\langle\Delta z_a(t)\rangle$, is determined via Eq. (43), leading to

$$\mathcal{L}\{\langle\Delta z_a(t)\rangle\}(\omega) = \frac{D_b}{D_r}\frac{\mu F}{(-i\omega)^2} + \frac{D_a}{D_r}\mathcal{L}\{\langle\Delta z(t)\rangle\}(\omega)$$
$$= \frac{\mu F}{(-i\omega)^2} + 2\pi n\sigma^3\frac{\mu F}{(-i\omega)^2}\frac{D_a}{D_r}\sum_{\ell=0}^{\infty} a_\ell\frac{\mathrm{i}'_\ell(\mathrm{Pe}/2)}{\mathrm{Pe}/2}. \tag{46}$$

By a one-sided Fourier transform of the time-dependent nonlinear mobility [Eq. (42)], we obtain the nonlinear frequency-dependent mobility $\hat{\mu}(\omega,\mathrm{Pe}) := -i\omega\mathcal{L}\{\langle\Delta z_a(t)\rangle\}(\omega)/F$ with

$$-i\omega\hat{\mu}(\omega,\mathrm{Pe})/\mu = 1 + 2\pi n\sigma^3\frac{D_a}{D_r}\sum_{\ell=0}^{\infty} a_\ell\frac{\mathrm{i}'_\ell(\mathrm{Pe}/2)}{\mathrm{Pe}/2}. \tag{47}$$

For the time-dependent case, we perform a numerical Fourier inversion of Eq. (47) and compare to event-driven Brownian-dynamics simulations at low density (Fig. 1). Initially, the probe particle experiences only the drag of the pure solvent, $\mu(t\to 0,\mathrm{Pe}) = \mu$. Then the dynamics slows down due to the interaction with the bath particles and approaches its stationary mobility $\mu(\mathrm{Pe}) := \mu(t\to\infty,\mathrm{Pe})$. Its dependence on the Péclet number is discussed in Sec. III C below.

In linear response, $\mathrm{Pe} = 0$, we recover the equilibrium solution [Eq. (49)] as anticipated by the fluctuation-dissipation theorem. In particular, for the equilibrium case, the approach to the stationary state is completely monotone and the time dependence can be worked out explicitly by Laplace inversion of Eq. (49) [38], leading to

$$\mu(t)/\mu = 1 - \frac{2\pi n\sigma^3}{3}\frac{D_a}{D_r}\{1-\cos(2t/\tau)[1-2\mathrm{C}(\sqrt{4t/\pi\tau})] - \sin(2t/\tau)[1-2\mathrm{S}(\sqrt{4t/\pi\tau})]\}, \tag{48}$$

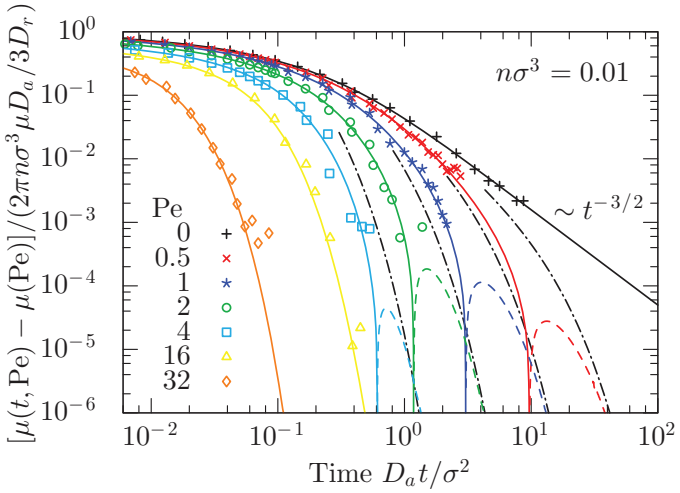


FIG. 1. Time-dependent approach of the mobility $\mu(t,\mathrm{Pe})$ to its stationary state for different Péclet numbers, Pe, and the linear response, $\mathrm{Pe}=0$. Solid lines represent the analytic solution and symbols correspond to Brownian-dynamics simulations for equal-sized colloids ($D_b = D_a$). Dashed lines indicate negative values. The black dash-dotted lines show the long-time behavior $\sim -t^{-3/2}\exp(-\mathrm{Pe}^2 D_a t/2\sigma^2)$ for the approach to the stationary state.

with Fresnel integrals $\mathrm{S}(x)=\int_0^x du\,\sin(\pi u^2/2)$ and $\mathrm{C}(x)=\int_0^x du\,\cos(\pi u^2/2)$ [50,51] and $\tau = \sigma^2/D_r$ is the diffusive time scale. Inserting the asymptotic expansions for the Fresnel integrals for large arguments, we recover the algebraic approach of $\sim t^{-3/2}$ to the stationary mobility which is due to repeated collisions of the probe particle with the same bath particle:

$$\mu(t)/\mu = 1 - \frac{2\pi n\sigma^3}{3}\frac{D_a}{D_r}\left\{1 - \frac{1}{4\sqrt{\pi}}(t/\tau)^{-3/2} + O(t^{-7/2})\right\}, \quad t\to\infty. \tag{49}$$

The persistent memory in the system also emerges as a long-time tail of the form $\sim t^{-5/2}$ in the velocity-autocorrelation function, $k_\mathrm{B}T\,d\mu(t)/dt$.

For finite driving, expansion of Eq. (47) yields

$$-i\omega\hat{\mu}(\omega,\mathrm{Pe})/\mu = 1 - 2\pi n\sigma^3\frac{D_a}{D_r}\left[1 - \frac{\mathrm{Pe}^2}{120} + \frac{\mathrm{Pe}^2}{8}\kappa\sigma - \frac{1}{2}(\kappa\sigma)^2 + \frac{1}{2}(\kappa\sigma)^3 + O(\mathrm{Pe}^4, \kappa^2\mathrm{Pe}^2, \kappa^4)\right], \tag{50}$$

which is analytic in the complex wave number $\kappa$ and the Péclet number. Moreover, only even terms in Pe appear. The nonanalytic dependence on the frequency and the Péclet number arises via the square root $\kappa\sigma = \sqrt{-i\omega\tau + (\mathrm{Pe}/2)^2}$. For vanishing forces $\kappa\sigma = \sqrt{-i\omega\tau}$ and the term $O(\kappa)^3$ generates the long-time tail in Eq. (49). For small but finite forces, the singularity is shifted in the complex plane and this term yields the long-time behavior in the time domain:

$$\frac{\mu(t,\mathrm{Pe})-\mu(\mathrm{Pe})}{2\pi n\sigma^3 D_a/3D_r} = \frac{1}{4\sqrt{\pi}}(t/\tau)^{-3/2}\exp(-\mathrm{Pe}^2 t/4\tau), \quad \mathrm{Pe}\to 0, \quad t\to\infty. \tag{51}$$

Therefore, the initial decay becomes more rapid and the long-time tail is followed only for small forces up to some driving-dependent crossover time $\tau_F := \tau/\mathrm{Pe}^2$, where the tail is decorated by a decaying exponential. Yet, there is a second nonanalytic contribution at finite driving $O(\mathrm{Pe}^2\kappa)$ (see also Ref. [36] for the corresponding lattice case), which yields in the temporal domain

$$\frac{\mu(t,\mathrm{Pe})-\mu(\mathrm{Pe})}{2\pi n\sigma^3 D_a/3D_r} = -\frac{1}{8\sqrt{\pi}}\,\mathrm{Pe}^2(t/\tau)^{-1/2}\exp(-\mathrm{Pe}^2 t/4\tau), \quad t\to\infty, \quad \mathrm{Pe}\to 0. \tag{52}$$

Comparing expressions in Eqs. (51) and (52) reveals that for times $t \gtrsim \tau_F = \tau/\mathrm{Pe}^2$ the latter decays more slowly and is the relevant one. Therefore, the divergent time scale $\tau_F$ in the problem separates two different regimes. For $t \lesssim \tau_F$ the linear response prediction remains qualitatively correct, while for $t \gtrsim \tau_F$ the nonequilibrium driving dominates. The second regime also explains the counterintuitive sign change in Fig. 1 such that in the terminal regime the velocity of the probe particle speeds up again for small and intermediate Péclet numbers. For large Péclet number the approach to the stationary state becomes monotonic again.

The simulations quantitatively confirm the theory for a low density of bath particles (see the Appendix for simulation details). Note that the simulations were performed at a finite density of $n\sigma^3 = 0.01$ (Fig. 1). Nevertheless, the agreement for the approach to the stationary behavior of the mobility extends to relative order $10^{-3}$. In particular, for equilibrium, we observe the persistent power-law correlations due to repeated interactions over roughly one decade in time.

### B. Fluctuations along the force

The next interesting quantity for the motion of the probe particle is the time-dependent fluctuation around the drift motion,

$$\mathrm{Var}_z(t) := \langle \Delta z_a(t)^2 \rangle - \langle \Delta z_a(t) \rangle^2, \tag{53}$$

which is the second cumulant of the fluctuating probe displacement $\Delta z_a(t)$. From the cumulant generating function [Eq. (41)], it is obtained via

$$\begin{aligned} \mathrm{Var}_z(t) &= -\frac{\partial^2}{\partial q^2} \ln \langle e^{-iq\Delta z_a(t)} \rangle = 2(D_a D_b/D_r)t - \frac{D_a^2}{D_r^2} \frac{\partial^2}{\partial (D_a q/D_r)^2} \ln \langle e^{-i(D_a q/D_r)\Delta z(t)} \rangle \\ &= 2(D_a D_b/D_r)t + \frac{D_a^2}{D_r^2} [\langle \Delta z(t)^2 \rangle - \langle \Delta z(t) \rangle^2], \end{aligned} \tag{54}$$

where, in the second line, we already inserted the explicit expression for the second cumulant of the relative displacement $\Delta z(t)$. First, we calculate the second moment along the field in the frequency domain:

$$\begin{aligned} \mathcal{L}\{\langle \Delta z(t)^2 \rangle\}(\omega) &= -\frac{\partial^2}{\partial q^2} G(q,\omega)|_{q=0} = \left[ -\frac{\partial^2 G_0}{\partial q^2} - 4G_0 \frac{\partial G_0}{\partial q} \frac{\partial \Sigma}{\partial q} - G_0^2 \frac{\partial^2 \Sigma}{\partial q^2} \right]_{q=0} \\ &= \frac{2D_r}{(-i\omega)^2} + \frac{2(\mu F)^2}{(-i\omega)^3} + 2\pi n\sigma^3 \frac{4(\mu F)^2}{(-i\omega)^3} \Delta\hat{\mu}(\omega, \mathrm{Pe}) + 2\pi n\sigma^3 \frac{4D_r}{(-i\omega)^2} \Delta\hat{R}(\omega, \mathrm{Pe}), \end{aligned} \tag{55}$$

where we introduce auxiliary functions

$$\Delta\hat{\mu}(\omega, \mathrm{Pe}) := \sum_{\ell=0}^{\infty} a_\ell \frac{\mathrm{i}_\ell'(\mathrm{Pe}/2)}{\mathrm{Pe}/2}, \tag{56}$$

$$\Delta\hat{R}(\omega, \mathrm{Pe}) := \sum_{\ell=0}^{\infty} \left[ \frac{i}{\sigma} \frac{\partial a_\ell}{\partial q} \mathrm{i}_\ell'(\mathrm{Pe}/2) + a_\ell \mathrm{i}_\ell''(\mathrm{Pe}/2) \right]. \tag{57}$$

In particular, with the auxiliary function for the mobility, $\Delta\hat{\mu}(\omega, \mathrm{Pe})$, the frequency-dependent nonlinear mobility [Eq. (47)] can be written as

$$-i\omega\hat{\mu}(\omega, \mathrm{Pe})/\mu = 1 + 2\pi n\sigma^3 \frac{D_a}{D_r} \Delta\hat{\mu}(\omega, \mathrm{Pe}). \tag{58}$$

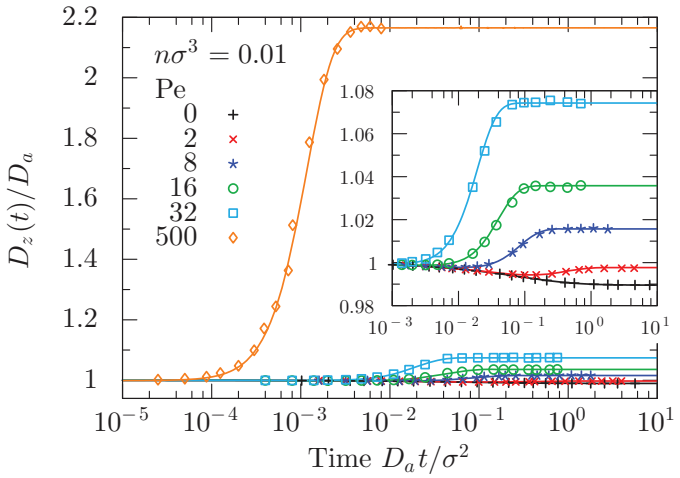


FIG. 2. Time-dependent diffusion coefficient $D_z(t)$ for different strength of the driving, $\mathrm{Pe} = \mu F \sigma / D_r$. Lines correspond to the analytic solution and symbols represent Brownian-dynamics simulation for equal-sized colloids ($D_b = D_a$). Inset: Zoom of the same quantity for the smaller Péclet numbers.

In the time domain, the mean-square displacement then follows as

$$\langle \Delta z(t)^2 \rangle = 2D_r t + (\mu F)^2 t^2 + 8\pi n\sigma^3 D_r \int_0^t dt'\, \mathcal{L}^{-1}\left\{ \frac{\Delta \hat{R}(\omega, \mathrm{Pe})}{(-i\omega)} + \frac{(\mu F)^2}{D_r} \frac{\Delta \hat{\mu}(\omega, \mathrm{Pe})}{(-i\omega)^2} \right\}(t'), \quad (59)$$

where we introduced the inverse Laplace transform $\mathcal{L}^{-1}\{\cdot\}(t)$. To calculate the square of the mean displacement $\langle \Delta z(t) \rangle$, we first express the frequency-dependent mean displacement given in Eq. (45) in the time domain leading to

$$\langle \Delta z(t) \rangle = \mu F t + 2\pi n\sigma^3 \mu F \int_0^t dt'\, \mathcal{L}^{-1}\left\{ \frac{\Delta \hat{\mu}(\omega, \mathrm{Pe})}{(-i\omega)} \right\}(t'). \quad (60)$$

Then, the square of the mean displacement to first order in the density is given by

$$\langle \Delta z(t) \rangle^2 = (\mu F)^2 t^2 + 4\pi n\sigma^3 (\mu F)^2 t \int_0^t dt'\, \mathcal{L}^{-1}\left\{ \frac{\Delta \hat{\mu}(\omega, \mathrm{Pe})}{(-i\omega)} \right\}(t') + O(n^2). \quad (61)$$

Collecting results, the time-dependent diffusion coefficient along the field, $D_z(t, \mathrm{Pe}) := (1/2) d\mathrm{Var}_z(t)/dt$, can be written as

$$D_z(t, \mathrm{Pe}) = D_a + 2\pi n\sigma^3 \frac{D_a^2}{D_r} \mathcal{L}^{-1}\left\{ \frac{2\Delta \hat{R}(\omega, \mathrm{Pe})}{(-i\omega)} + \frac{\mathrm{Pe}^2}{(-i\omega)} \frac{\partial \Delta \hat{\mu}(\omega, \mathrm{Pe})}{\partial(-i\omega\tau)} \right\}(t), \quad (62)$$

where we used the relation $t\mathcal{L}^{-1}\{(\cdot)\}(t) = \mathcal{L}^{-1}\{\partial(\cdot)/\partial(-i\omega)\}(t)$ of the Laplace transform.

For small times the probe particle does not interact with the bath particles and the diffusion coefficient is given by the bare one, $D_z(t \to 0, \mathrm{Pe}) = D_a$. Only in the equilibrium case, the diffusion coefficient decreases monotonically (see Fig. 2) to its stationary-state value $D_z^{\mathrm{eq}}/D = 1 - (D_a/D_r) 2\pi n\sigma^3/3$.

For any finite driving, a minimum of least diffusivity emerges at intermediate times such that the growth of the fluctuations speeds up again until the stationary diffusion coefficient is reached (Fig. 2 inset). With increasing driving the time of least diffusivity becomes smaller and smaller. The time-dependent growth becomes arbitrarily large as the Péclet number is increased, even at small densities. A growing time-dependent diffusion coefficient is a fingerprint of transient superdiffusive behavior.

The superdiffusion becomes more and more pronounced upon increasing the force beyond values that are feasible for numerical implementation of our analytical solution ($\mathrm{Pe} \gtrsim 10^3$). Nevertheless,

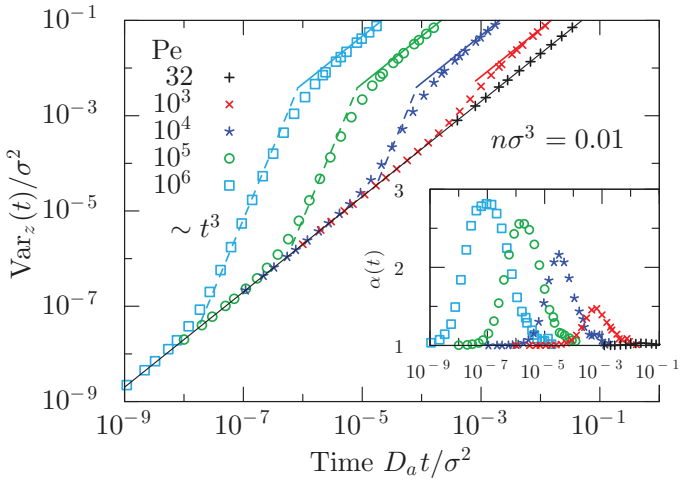


FIG. 3. Time-dependent fluctuations $\mathrm{Var}_z(t) = \langle \Delta z_a(t)^2 \rangle - \langle \Delta z_a(t) \rangle^2$ and local exponent $\alpha(t) = d\ln[\mathrm{Var}_z(t)]/d\ln(t)$ (inset) of the probe particle along the applied force obtained from Brownian-dynamics simulation of equal-sized colloids ($D_b = D_a$) for different strength of the driving. The solid lines correspond to the diffusive asymptote $\mathrm{Var}_z(t) = 2D_z(\mathrm{Pe})t$ and the dashed lines are the asymptotic model $\mathrm{Var}_z(t) = (D_a/D_r)^2(\mu F t)^3/3l_*$ with the empirical mean-free path length $l_* \approx 1/n\sigma^2$.

in simulations the regime of these large Péclet numbers can still be accessed (Fig. 3). The window of superdiffusion opens for stronger driving and the local exponent for the variance

$$\alpha(t) := \frac{d\ln[\mathrm{Var}_z(t)]}{d\ln(t)} = \frac{2D_z(t, \mathrm{Pe})t}{\mathrm{Var}_z(t)} \tag{63}$$

approaches a value of 3 at intermediate times. The long-time behavior is for all forces diffusive with a strongly enhanced diffusion coefficient $D_z(\mathrm{Pe})/D \simeq \pi n\sigma^3 \mathrm{Pe}[\ln(2) - 1/4]/6$, for $\mathrm{Pe} \to \infty$ [4].

Let us rationalize the superdiffusive behavior in terms of an asymptotic model for the limit of strong driving. Therefore, we adapt an earlier asymptotic model valid for the driven lattice Lorentz model [35]. Here, the probe particle's motion is dominated by the drift with constant velocity $\mu F$ along the force until it hits a bath particle for the first time and then slowly slides along its surface. In this time regime, the motion becomes essentially one-dimensional such that the probability distribution for the relative motion, $\mathbb{P}(\Delta z, t)$, consists of freely moving particles with fixed velocity or particles that are transiently blocked by bath particles. The free path lengths are exponentially distributed, since at low density the positions of the bath particles are independent, and the probability distribution can be estimated directly to

$$\mathbb{P}(\Delta z, t) = \delta(\Delta z - vt)e^{-\Delta z/l_*} + (1/l_*)e^{-\Delta z/l_*}\vartheta(vt - \Delta z), \tag{64}$$

where $l_* = 1/n\Sigma_*$ denotes a mean-free path length. The first term corresponds to the freely moving probe (with $v = \mu F$), while the second term accounts for the blocked probe particles.

From the distribution of the displacements [Eq. (64)], it is straightforward to calculate the mean and the mean-square displacement. Then, the growth of the fluctuations for the probe particle is obtained from Eq. (54), where we discarded the diffusive contribution since we are only interested in the drift motion. As a result, the distribution of the displacements implies a strong initial growth of the variance with

$$\mathrm{Var}_z(t) = \left(\frac{D_a}{D_r}\right)^2 \frac{(\mu F t)^3}{3l_*}, \tag{65}$$

which is also confirmed by Brownian-dynamics simulation (Fig. 3). Empirically we find that the relevant scattering cross section $\Sigma_* \approx \sigma^2$ is smaller than the geometric cross section $\pi\sigma^2$, leading to a mean-free path length of $l_* \approx 1/n\sigma^2$. The smaller scattering cross section can be

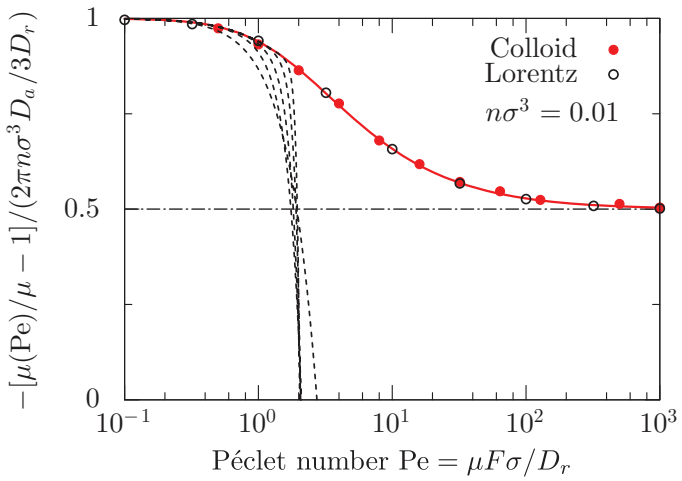


FIG. 4. Density-induced suppression of the stationary mobility $\mu(\mathrm{Pe})$. Dashed lines indicate the asymptotic expansion for increasing order (2, 4, 6, 10, and 20). Lines correspond to the theory and symbols represent Brownian-dynamics simulations of equal-sized colloids, $D_b = D_a$, and Lorentz systems with $D_b = 0$.

readily interpreted since only head-on collisions effectively stop the directed motion (in the lattice variant no empirical correction was necessary; the scattering cross section coincides with the geometrical one [35]). Matching the superdiffusion with the short-time asymptote $2D_a t$ yields as crossover time $\sim \mathrm{Pe}^{-3/2}$. Similarly the terminal time of superdiffusion is set by the time the probe particle needs to pass a bath particle $\sigma/\mu F \sim 1/\mathrm{Pe}$ leading by crossover matching to the scaling prediction $D_z(\mathrm{Pe}) \sim n\,\mathrm{Pe}$ for the diffusion coefficient consistent with Ref. [4]. Thus, the window of superdiffusion expands as $\mathrm{Pe}^{1/2}$ as the force is increased.

### C. Long-time behavior

Let us specialize our time-dependent solution to the stationary state. The stationary mobility $\mu(\mathrm{Pe})$ follows as a special case from Eq. (47) via

$$\mu(\mathrm{Pe})/\mu = \lim_{\omega\to 0}(-i\omega)\hat{\mu}(\omega,\mathrm{Pe})/\mu = 1 + 2\pi n\sigma^3\frac{D_a}{D_r}\Delta\mu_0(\mathrm{Pe}), \tag{66}$$

where the coefficient $\Delta\mu_0(\mathrm{Pe})$ is defined via a low-frequency expansion of the auxiliary function

$$\Delta\hat{\mu}(\omega,\mathrm{Pe}) = \Delta\mu_0(\mathrm{Pe}) + (-i\omega\tau)\Delta\mu_1(\mathrm{Pe}) + \cdots, \quad \omega\to 0. \tag{67}$$

For small driving and small frequency, we can determine the coefficients $a_\ell$ of the auxiliary function $\Delta\hat{\mu}(\omega,\mathrm{Pe})$ [Eq. (56)] by an inversion of the tridiagonal matrix equation [Eq. (32)] and by considering the frequency-independent contribution:

$$\Delta\mu_0(\mathrm{Pe}) = -\frac{1}{3} + \frac{2}{45}\mathrm{Pe}^2 - \frac{1}{24}|\mathrm{Pe}|^3 + \frac{128}{4725}\mathrm{Pe}^4 + O(|\mathrm{Pe}|^5), \quad \mathrm{Pe}\to 0. \tag{68}$$

Inserting this result into Eq. (66), we recover the previously derived asymptotic expansion [Eq. (1)] [1]. In particular, in equilibrium, $\Delta\mu_0(\mathrm{Pe}\to 0) = -1/3$ and for equal-sized colloids with relative diffusion coefficient $D_r = 2D_a$ and packing fraction $\varphi = \pi n\sigma^3/6$, we obtain the known result from equilibrium, $\mu(\mathrm{Pe}=0)/\mu = 1 - 2\varphi$ [37]. In the limit of large forces, $\mathrm{Pe}\to\infty$, the analytic solution for the mobility [Eq. (66)] approaches the limit $\mu(\mathrm{Pe}\to\infty)/\mu = 1 - (D_a/D_r)\pi n\sigma^3/3$ (Fig. 4), derived earlier in terms of a boundary layer analysis [1].

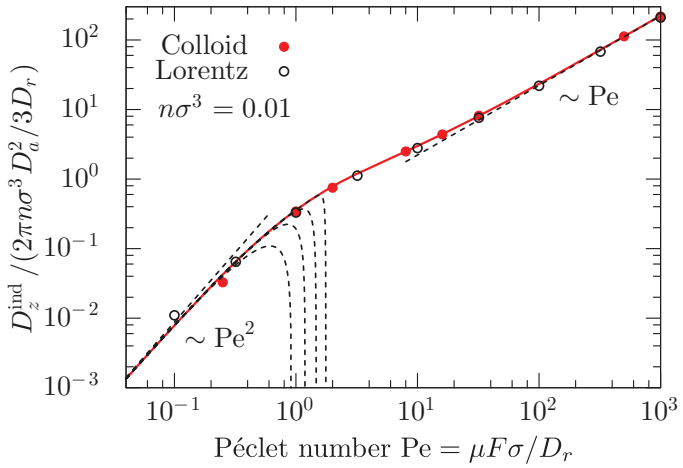


FIG. 5. Stationary-state force-induced diffusion coefficient $D_z^{\mathrm{ind}} := D_z(\mathrm{Pe}) - D_z(\mathrm{Pe} \to 0)$. Dashed lines represent the asymptotic behavior for small (increasing order 2, 3, 5, 9, and 31) and large driving. Lines correspond to the theory and symbols represent Brownian-dynamics simulations of equal-sized colloids, $D_b = D_a$, and Lorentz systems $D_b = 0$.

Similarly, for the stationary diffusion coefficient $D_z(\mathrm{Pe})$, we perform the limit of small frequencies in Eq. (62) and obtain

$$D_z(\mathrm{Pe})/D_a = \lim_{\omega\to 0}(-i\omega)\hat{D}_z(\omega,\mathrm{Pe})/D_a = 1 + 2\pi n\sigma^3\frac{D_a}{D_r}[2\Delta R_0(\mathrm{Pe}) + \mathrm{Pe}^2\Delta\mu_1(\mathrm{Pe})], \tag{69}$$

where the coefficient $\Delta\mu_1(\mathrm{Pe})$ is defined in Eq. (67) and the coefficient $\Delta R_0(\mathrm{Pe}) := \Delta\hat{R}(\omega \to 0, \mathrm{Pe})$ is the small-frequency limit of the auxiliary function $\Delta\hat{R}(\omega, \mathrm{Pe})$ [Eq. (57)]. Similar to the coefficient $\Delta\mu_0(\mathrm{Pe})$, we determine the coefficients $a_\ell$ and $\partial a_\ell/\partial q$ by matrix inversion of the tridiagonal matrix equation [Eq. (32)] in powers of the Péclet number and the frequency. The coefficients are then obtained as

$$\Delta R_0(\mathrm{Pe}) = -\frac{1}{6} + \frac{17}{270}\mathrm{Pe}^2 - \frac{11}{144}|\mathrm{Pe}|^3 + \frac{1679}{28350}\mathrm{Pe}^4 + O(|\mathrm{Pe}|)^5, \quad \mathrm{Pe}\to 0, \tag{70}$$

$$\Delta\mu_1(\mathrm{Pe}) = \frac{1}{6} - \frac{1}{6}|\mathrm{Pe}| + \frac{101}{810}\mathrm{Pe}^2 - \frac{17}{216}|\mathrm{Pe}|^3 + \frac{310571}{6804000}\mathrm{Pe}^4 + O(|\mathrm{Pe}|)^5, \quad \mathrm{Pe}\to 0, \tag{71}$$

and the series expansion of the diffusion coefficient parallel to the applied field is calculated to

$$D_z(\mathrm{Pe})/D_a = 1 - \frac{2\pi n\sigma^3}{3}\frac{D_a}{D_r}\left[1 - \frac{79}{90}\mathrm{Pe}^2 + \frac{23}{24}|\mathrm{Pe}|^3 - \frac{6893}{9450}\mathrm{Pe}^4 + O(|\mathrm{Pe}|)^5\right]. \tag{72}$$

With our solution, we recover the leading correction $O(\mathrm{Pe}^2)$ to the equilibrium case, which was calculated earlier [4]. Furthermore, our calculation extends this result to arbitrary order and reveals the emergence of nonanalytic contributions similar to the mobility in the stationary state.

As can be inferred from the stationary mobility (Fig. 4) and the stationary diffusion coefficient (Fig. 5), both series expansions [Eqs. (1) and (72)] break down already at moderate driving. However, the numerical evaluation via the matrix inversion [Eq. (32)] is valid for the full range of Péclet numbers, which was shown first by Khair and Brady [2] for the mobility. The limiting value of the stationary mobility as well as the asymptotic behavior $O(\mathrm{Pe})$ of the stationary diffusion coefficient for large Péclet numbers (Fig. 5) [4] is nicely corroborated in the Brownian-dynamics simulations.

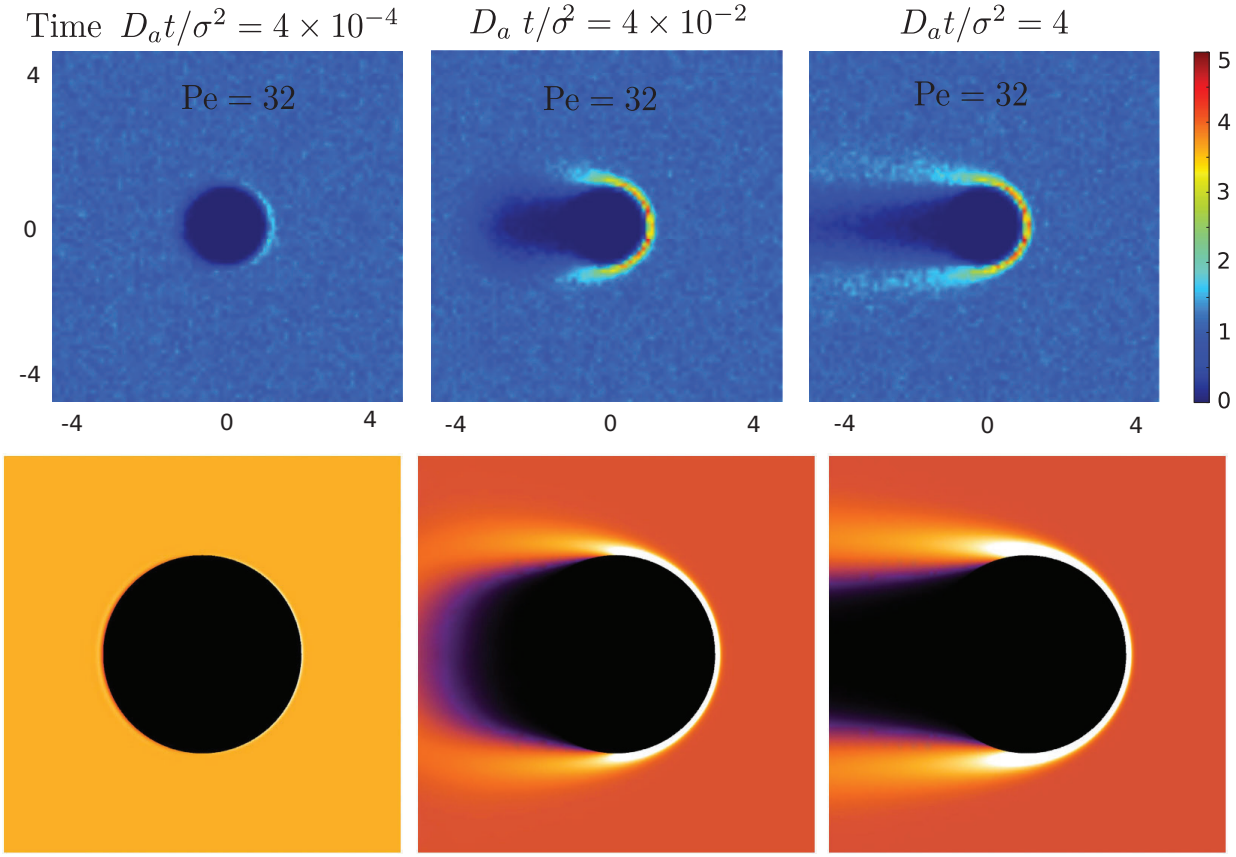


FIG. 6. Top: Simulation results for the time-dependent pair-distribution function $g(\vec{r}, t)$ for Péclet number $\mathrm{Pe} = 32$ and density $n\sigma^3 = 0.01$. As time progresses, $t D_a/\sigma^2 = 4 \times 10^{-4}, 4 \times 10^{-2}, 4$ (left to right), the tracer piles up probability in front and leaves a trail of depleted probability. Bottom: Analytic result for the real part of the pair-distribution function in the frequency domain $\mathrm{Re}[-i\omega\hat{g}(\vec{r}, \omega)]$ at the same driving $\mathrm{Pe} = 32$ for frequencies $\omega\sigma^2/2\pi D_a = 1/(4 \times 10^{-4}), 1/(4 \times 10^{-2}), 1/4$ (left to right).

### D. Time-dependent pair-distribution function

Our solution provides also the time-dependent pair-distribution function $g(\vec{r}, t)$ for the relative distance $\vec{r}$ of the tracer and the bath particles by integrating the conditional probability distribution $\psi(\vec{r}, t|\vec{r}')$ over all $\vec{r}'$. In the frequency domain, $\hat{g}(\vec{r}, \omega) = \hat{\psi}_{q=0}(\vec{r}, \omega)\sqrt{V}$ and with Eq. (28), we find for $|\vec{r}| > \sigma$

$$-i\omega\hat{g}(\vec{r}, \omega) = 1 + e^{\mu\vec{F}\cdot\vec{r}/2D_r} \sum_{\ell=0}^{\infty} a_\ell \frac{\mathrm{k}_\ell(\kappa r)}{\mathrm{k}_\ell(\kappa\sigma)} \mathrm{P}_\ell(\cos\vartheta), \tag{73}$$

where the coefficients $a_\ell \equiv a_\ell(q\sigma, \kappa\sigma, \mathrm{Pe})$ are to be evaluated at zero wave number $q = 0$. In particular, in equilibrium all coefficients vanish ($a_\ell = 0$) and the pair-distribution function reduces to the stationary step function.

Simulation results for the time evolution of the pair-distribution function are displayed in Fig. 6. Shortly after switching on the force, the pair-distribution function is still almost spherically symmetric; there has been no time to propagate the information of the strong perturbing force to the surroundings. Quickly the tracer's motion is obstructed by the bath particles such that probability accumulates in front of the tracer particle. For longer times, a trailing wake evolves where probability is depleted behind the tracer particle. The numerical results for the pair-distribution function in the frequency domain shown in Fig. 6 corroborate this picture. For small frequencies we recover the stationary distribution calculated in Refs. [1,2]. For high Péclet numbers the stationary two-particle distribution function becomes strongly asymmetric as was shown first Ref. [1] and

more systematically in Ref. [2]. Probability piles up in a narrow boundary layer in front of the pulled particle and leaves behind a wake extending to larger and larger distances $O(\mathrm{Pe})$ as the driving force is increased.

## IV. SUMMARY AND CONCLUSION

We have derived an analytic solution for the full time-dependent response of a probe particle driven out of equilibrium by a step force in first order of the density of bath particles (discarding inertial and hydrodynamic effects). The response is completely encoded in the self-energy from which, in principle, all moments along the force can be generated. In comparison to the known self-energy in equilibrium, the force results in a complex shift of the frequency $-i\omega\tau \mapsto -i\omega\tau + (\mathrm{Pe}/2)^2 = \kappa^2\sigma^2$ encoded in the complex wave number $\kappa\sigma$, an explicit regular variation of the expansion coefficients $a_\ell$ via the boundary condition, and a shift in the wave number $q\sigma \mapsto q\sigma + i\,\mathrm{Pe}/2$. The shift in the frequency reveals that the nonanalytic frequency behavior in equilibrium, as manifested in the long-time tails, and the nonanalytic dependence on the driving are merely two sides of the same coin. In particular, this explains why at any finite driving the approach of the nonlinear mobility to its stationary value becomes exponentially fast. Furthermore, this reveals that, for finite times, all response functions are analytic functions in the driving; however, this does not hold for infinite times since the limits do not commute.

The emergence of nonanalytic behavior and a divergent time scale for $\mathrm{Pe} \to 0$ calls for an explanation in terms of physics. The stationary Smoluchowski equation is nonuniform at small Péclet number (the same physics has been discussed for the advection-diffusion equation in the seminal contribution by Acrivos and Taylor [52]): it displays an outer region at distances $r \gg \sigma/\mathrm{Pe}$ where advection dominates, and an inner one where diffusion is the dominant contribution. For the transport coefficient already to order $O(\mathrm{Pe}^2)$ both regions need to be calculated and matching the solutions makes the nonanalytic contributions evident [2]. For nonzero frequencies or finite times the advected Smoluchowski equation is regular and solutions decay exponentially fast on the "skin penetration" depth $\sqrt{D_r/\omega} \sim \sqrt{D_r t}$. Correspondingly, if the skin penetration depth is smaller than the inner region, i.e., for times $\sqrt{D_r t}, \lesssim \sigma/\mathrm{Pe}$, i.e., $t \lesssim \tau_F = \tau/\mathrm{Pe}^2$, one can safely ignore the presence of the outer region and the system behaves as in linear response. In contrast, for large enough times, the skin penetration depth covers the outer region and the nonlinearities become important. The interplay of the divergent boundary layer and the skin penetration depth is the origin of noncommuting limits. Mathematically related, but not quite identical, is the problem of the time-dependent motion at small but finite Reynolds number [53].

The full solution provides the first direct access to the time-dependent fluctuations along the force. Here we explicitly characterized the transient superdiffusion which connects the short-time bare diffusion and the long-time enhanced diffusion [4]. The emergence of superdiffusion has been rationalized by considering the distribution of the free path lengths.

Let us comment also on hydrodynamic interactions. Progress has been made for certain limiting cases: In equilibrium, the stationary diffusion coefficients have been estimated by including instantaneous hydrodynamic interactions at the level of the Oseen tensor, as well as including near-field corrections. Results for the density-induced suppression depend somewhat on the approximation of the hydrodynamic interactions but are close to the diffusion coefficient neglecting hydrodynamics [37,54–56]. For the driven case, hydrodynamic interactions have been accounted for in the stationary state for both the structure deformation as well as the mobility for all Péclet numbers [41]. The force-induced corrections to the stationary diffusion coefficient have been elaborated only recently, and it has been shown that hydrodynamic interactions do not lead to qualitatively new behavior, although the numerical values change. In particular, the low-force corrections are still $O(\mathrm{Pe}^2)$, and in the regime of strong forces they still scale as $O(\mathrm{Pe})$, however with a slow convergence to the asymptotic result [56].

A second effect due to hydrodynamics arises due to frequency-dependent hydrodynamic interactions implying hydrodynamic memory. Here, the slow vortex diffusion of transverse momentum

in the fluid leads to a characteristic algebraic decay of the form $\simeq Bt^{-3/2}$, $B > 0$, for the velocity-autocorrelation function of the particle [57,58]. Hence, one may ask the question if the long-time tail due to hydrodynamics dominates the long-time tail $\simeq -At^{-5/2}$, $A > 0$, due to repeated collisions of the probe particle with the bath particles. Taking physical values from experiments [59,60] and comparing both tails shows that, in principle, a window of time opens where the algebraic decay due to the collision of the probe particle with bath particles dominates before hydrodynamics becomes relevant at larger times.

Our predictions for the time-dependent response of a driven colloid can be tested, in principle, in laboratory experiments on a colloidal suspension via particle tracking. The general scenario persists also for soft spheres and is not restricted to dilute systems. To first order in the density, the different diffusivities of probe and bath particles can be trivially accounted for, e.g., by a rescaling of time. In particular, the case of a dilute and quenched array of obstacles (Lorentz model) is also included. Simulation of the Lorentz model, where the bath particles are pinned, was added to the comparison of the mobility and diffusivity with theory in Figs. 4 and 5.

Our analysis of the driven colloid shows that the nonequilibrium stationary state is inherently a nonanalytic function of the driving such that the transport coefficients cannot be expanded in a Taylor series beyond linear response. Although this has been derived to first order in the densities only, this behavior is anticipated to be generic and valid for arbitrary densities. Arguably, such relations should hold universally in a general nonlinear response framework. This view is supported by recent predictions for a two-dimensional or three-dimensional driven lattice Lorentz gas [34–36], where qualitatively the same scenario applies.

## ACKNOWLEDGMENTS

We gratefully acknowledge support by the Deutsche Forschungsgemeinschaft (DFG) research unit FOR1394 "Nonlinear response to probe vitrification" and European Regional Development Funds (ERDF) and MINECO under Project No. FIS2015-69022P (AMP). The computational results presented have been achieved (in part) using the HPC infrastructure LEO of the University of Innsbruck. The collaboration has greatly benefitted from COST MP1305 flowing matter.

## APPENDIX: COMPUTER SIMULATIONS

We have simulated the motion of the pulled probe particle in the presence of bath particles interacting via a hard-core potential using event-driven pseudo-Brownian-dynamics simulation [61] ignoring inertial effects or hydrodynamic interactions. The starting point for the stochastic simulation of the suspension is the Langevin equation

$$d\vec{r} = \sqrt{2D_a}\vec{\eta}(t)dt + \mu F\vec{e}_z dt, \tag{A1}$$

which describes the change of position $d\vec{r}$ of the probe particle in terms of the Gaussian white noise process $\vec{\eta}$ with zero mean and covariance $\langle \eta_i(t)\eta_j(t)\rangle = \delta_{ij}\delta(t-t')$. For the bath particles, the same equation with $F = 0$ holds. The Langevin equation [Eq. (A1)] is implemented by introducing a fixed Brownian time step $\tau_B$, such that for every step, the pseudovelocity

$$\vec{v} = \sqrt{\frac{2D_a}{\tau_B}}\mathcal{N}_\eta + \mu F\vec{e}_z \tag{A2}$$

is assigned to the probe and the bath particles ($F = 0$). Between these Brownian interrupts the particles move with constant velocities and collide elastically [61]. The normal distributed random variable $\mathcal{N}_\eta$ arises from discretization of the white noise and has zero mean and unit variance. The Brownian time step $\tau_B$ should be much smaller than the diffusion time $\sigma^2/D_a$ and the drift time $\sigma/\mu F$.

For the colloidal case, we have used equilibrated configurations consisting of 1000 particles at a fixed number density $n\sigma^3 = 0.01$, and a typical value of the Brownian time step is $\tau_B \simeq 10^{-3}(\sigma^2/D_a)/\max(1, \mathrm{Pe})$. For each data set, we have simulated at least $10^7$ independent trajectories. For the case of the Lorentz system, we freeze the dynamics of the bath particles and apply the stochastic dynamics only to the tracer particle.


[1] T. M. Squires and J. F. Brady, A simple paradigm for active and nonlinear microrheology, Phys. Fluids **17**, 073101 (2005).

[2] A. S. Khair and J. F. Brady, Single particle motion in colloidal dispersions: A simple model for active and nonlinear microrheology, J. Fluid Mech. **557**, 73 (2006).

[3] L. G. Wilson, A. W. Harrison, A. B. Schofield, J. Arlt, and W. C. K. Poon, Passive and active microrheology of hard-sphere colloids, J. Phys. Chem. B **113**, 3806 (2009).

[4] R. N. Zia and J. F. Brady, Single-particle motion in colloids: Force-induced diffusion, J. Fluid Mech. **658**, 188 (2010).

[5] I. Sriram, A. Meyer, and E. M. Furst, Active microrheology of a colloidal suspension in the direct collision limit, Phys. Fluids **22**, 062003 (2010).

[6] L. G. Wilson and W. C. K. Poon, Small-world rheology: An introduction to probe-based active microrheology, Phys. Chem. Chem. Phys. **13**, 10617 (2011).

[7] R. N. Zia and J. F. Brady, Microviscosity, microdiffusivity, and normal stresses in colloidal dispersions, J. Rheol. **56**, 1175 (2012).

[8] J. W. Swan and R. N. Zia, Active microrheology: Fixed-velocity versus fixed-force, Phys. Fluids **25**, 083303 (2013).

[9] A. M. Puertas and Th. Voigtmann, Microrheology of colloidal systems, J. Phys.: Condens. Matter **26**, 243101 (2014).

[10] R. N. Zia and J. F. Brady, Theoretical microrheology, in *Complex Fluids in Biological Systems: Experiment, Theory, and Computation*, edited by E. S. Spagnolie (Springer, New York, 2015), pp. 113–157.

[11] E. M. Furst and T. M. Squires, *Microrheology* (Oxford University Press, Oxford, 2017).

[12] D. Winter, J. Horbach, P. Virnau, and K. Binder, Active Nonlinear Microrheology in a Glass-Forming Yukawa Fluid, Phys. Rev. Lett. **108**, 028303 (2012).

[13] D. Winter and J. Horbach, Nonlinear active micro-rheology in a glass-forming soft-sphere mixture, J. Chem. Phys. **138**, 12A512 (2013).

[14] I. Gazuz, A. M. Puertas, Th. Voigtmann, and M. Fuchs, Active and Nonlinear Microrheology in Dense Colloidal Suspensions, Phys. Rev. Lett. **102**, 248302 (2009).

[15] M. V. Gnann, I. Gazuz, A. M. Puertas, M. Fuchs, and Th. Voigtmann, Schematic models for active nonlinear microrheology, Soft Matter **7**, 1390 (2011).

[16] M. V. Gnann and Th. Voigtmann, Asymptotic analysis of mode-coupling theory of active nonlinear microrheology, Phys. Rev. E **86**, 011406 (2012).

[17] Ch. J. Harrer, D. Winter, J. Horbach, M. Fuchs, and Th. Voigtmann, Force-induced diffusion in microrheology, J. Phys.: Condens. Matter **24**, 464105 (2012).

[18] I. Gazuz and M. Fuchs, Nonlinear microrheology of dense colloidal suspensions: A mode-coupling theory, Phys. Rev. E **87**, 032304 (2013).

[19] T. Wang, M. Grob, A. Zippelius, and M. Sperl, Active microrheology of driven granular particles, Phys. Rev. E **89**, 042209 (2014).

[20] M. Gruber, G. C. Abade, A. M. Puertas, and M. Fuchs, Active microrheology in a colloidal glass, Phys. Rev. E **94**, 042602 (2016).

[21] R. L. Jack, D. Kelsey, J. P. Garrahan, and D. Chandler, Negative differential mobility of weakly driven particles in models of glass formers, Phys. Rev. E **78**, 011506 (2008).

[22] C. F. E. Schroer and A. Heuer, Anomalous Diffusion of Driven Particles in Supercooled Liquids, Phys. Rev. Lett. **110**, 067801 (2013).

[23] C. F. E. Schroer and A. Heuer, Microrheology of supercooled liquids in terms of a continuous time random walk, J. Chem. Phys. **138**, 12A518 (2013).
[24] R. Burioni, G. Gradenigo, A. Sarracino, A. Vezzani, and A. Vulpiani, Scaling properties of field-induced superdiffusion in continuous time random walks, Commun. Theor. Phys. **62**, 514 (2014).
[25] V. Démery, O. Bénichou, and H. Jacquin, Generalized Langevin equations for a driven tracer in dense soft colloids: Construction and applications, New J. Phys. **16**, 053032 (2014).
[26] V. Démery, Mean-field microrheology of a very soft colloidal suspension: Inertia induces shear thickening, Phys. Rev. E **91**, 062301 (2015).
[27] T. Wang and M. Sperl, Thinning and thickening in active microrheology, Phys. Rev. E **93**, 022606 (2016).
[28] O. Bénichou, A. Bodrova, D. Chakraborty, P. Illien, A. Law, C. Mejía-Monasterio, G. Oshanin, and R. Voituriez, Geometry-Induced Superdiffusion in Driven Crowded Systems, Phys. Rev. Lett. **111**, 260601 (2013).
[29] P. Illien, O. Bénichou, C. Mejía-Monasterio, G. Oshanin, and R. Voituriez, Active Transport in Dense Diffusive Single-File Systems, Phys. Rev. Lett. **111**, 038102 (2013).
[30] O. Bénichou, P. Illien, C. Mejía-Monasterio, and G. Oshanin, A biased intruder in a dense quiescent medium: Looking beyond the force-velocity relation, J. Stat. Mech.: Theory Exp. (2013) P05008.
[31] O. Bénichou, P. Illien, G. Oshanin, A. Sarracino, and R. Voituriez, Microscopic Theory for Negative Differential Mobility in Crowded Environments, Phys. Rev. Lett. **113**, 268002 (2014).
[32] P. Illien, O. Bénichou, G. Oshanin, and R. Voituriez, Velocity Anomaly of a Driven Tracer in a Confined Crowded Environment, Phys. Rev. Lett. **113**, 030603 (2014).
[33] P. Illien, O. Bénichou, G. Oshanin, and R. Voituriez, Distribution of the position of a driven tracer in a hardcore lattice gas, J. Stat. Mech. (2015) P11016.
[34] S. Leitmann and T. Franosch, Nonlinear Response in the Driven Lattice Lorentz Gas, Phys. Rev. Lett. **111**, 190603 (2013).
[35] S. Leitmann and T. Franosch, Time-Dependent Fluctuations and Superdiffusivity in the Driven Lattice Lorentz Gas, Phys. Rev. Lett. **118**, 018001 (2017).
[36] S. Leitmann, O. Bénichou, and T. Franosch, Time-dependent dynamics of the three-dimensional driven lattice Lorentz gas, J. Phys. A: Math. Theor. **51**, 375001 (2018).
[37] S. Hanna, W. Hess, and R. Klein, Self-diffusion of spherical Brownian particles with hard-core interaction, Phys. A (Amsterdam, Neth.) **111**, 181 (1982).
[38] S. Hanna, W. Hess, and R. Klein, The velocity autocorrelation function of an overdamped Brownian system with hard-core intraction, J. Phys. A **14**, L493 (1981).
[39] B. J. Ackerson and L. Fleishman, Correlations for dilute hard core suspensions, J. Chem. Phys. **76**, 2675 (1982).
[40] B. U. Felderhof and R. B. Jones, Diffusion in hard sphere suspensions, Phys. A (Amsterdam, Neth.) **122**, 89 (1983).
[41] A. S. Khair and J. F. Brady, Microviscoelasticity of colloidal dispersions, J. Rheol. **49**, 1449 (2005).
[42] M. H. Ernst and A. Weyland, Long time behaviour of the velocity auto-correlation function in a Lorentz gas, Phys. Lett. A **34**, 39 (1971).
[43] H. van Beijeren, Transport properties of stochastic Lorentz models, Rev. Mod. Phys. **54**, 195 (1982).
[44] Th. M. Nieuwenhuizen, P. F. J. van Velthoven, and M. H. Ernst, Diffusion and Long-Time Tails in a Two-Dimensional Site-Percolation Model, Phys. Rev. Lett. **57**, 2477 (1986).
[45] F. Höfling and T. Franosch, Crossover in the Slow Decay of Dynamic Correlations in the Lorentz Model, Phys. Rev. Lett. **98**, 140601 (2007).
[46] T. Franosch, F. Höfling, T. Bauer, and E. Frey, Persistent memory for a Brownian walker in a random array of obstacles, Chem. Phys. **375**, 540 (2010).
[47] T. Bauer, F. Höfling, T. Munk, E. Frey, and T. Franosch, The localization transition of the two-dimensional Lorentz model, Eur. Phys. J. Spec. Top. **189**, 103 (2010).
[48] B. U. Felderhof and R. B. Jones, Cluster expansion of the diffusion kernel of a suspension of interacting Brownian particles, Phys. A (Amsterdam, Neth.) **121**, 329 (1983).
[49] D. R. Nelson and N. M. Shnerb, Non-Hermitian localization and population biology, Phys. Rev. E **58**, 1383 (1998).

[50] *NIST Handbook of Mathematical Functions*, edited by F. W. J. Olver, D. W. Lozier, R. F. Boisvert, and C. W. Clark (Cambridge University Press, New York, 2010), print companion to Ref. [51] .
[51] DLMF, NIST Digital Library of Mathematical Functions, http://dlmf.nist.gov/, Release 1.0.15, online companion to Ref. [50] .
[52] A. Acrivos and T. D. Taylor, Heat and mass transfer from single spheres in Stokes flow, Phys. Fluids **5**, 387 (1962).
[53] P. M. Lovalenti and J. F. Brady, The hydrodynamic force on a rigid particle undergoing arbitrary time-dependent motion at small Reynolds number, J. Fluid Mech. **256**, 561 (1993).
[54] G. K. Batchelor, Brownian diffusion of particles with hydrodynamic interaction, J. Fluid Mech. **74**, 1 (1976).
[55] J. M. Rallison and E. J. Hinch, The effect of particle interactions on dynamic light scattering from a dilute suspension, J. Fluid Mech. **167**, 131 (1986).
[56] N. J. Hoh and R. N. Zia, Force-induced diffusion in suspensions of hydrodynamically interacting colloids, J. Fluid Mech. **795**, 739 (2016).
[57] B. J. Alder and T. E. Wainwright, Decay of the velocity autocorrelation function, Phys. Rev. A **1**, 18 (1970).
[58] R. Zwanzig and M. Bixon, Hydrodynamic theory of the velocity correlation function, Phys. Rev. A **2**, 2005 (1970).
[59] T. Franosch, M. Grimm, M. Belushkin, F. M. Mor, G. Foffi, L. Forró, and S. Jeney, Resonances arising from hydrodynamic memory in Brownian motion, Nature (London) **478**, 85 (2011).
[60] S. Jeney, B. Lukić, J. A. Kraus, T. Franosch, and L. Forró, Anisotropic Memory Effects in Confined Colloidal Diffusion, Phys. Rev. Lett. **100**, 240604 (2008).
[61] A. Scala, Th. Voigtmann, and C. De Michele, Event-driven Brownian dynamics for hard spheres, J. Chem. Phys. **126**, 134109 (2007).